A Single Vortex in a Bose-Einstein Condensate

Bachelor Thesis by
Nikolas Zöller

Supervisor: Priv.-Doz. Dr. Axel Pelster

August 11th, 2010

Department of Physics
Freie Universität Berlin
Arnimallee 14
14195 Berlin, Germany

Contents

1 Introduction

The derivation of the quantum statistics of bosons by Satyendra Nath Bose [1] and the adjacent investigations of Albert Einstein in 1924 [2] led to the prediction of a phase transition to a new quantum state of matter at very low temperatures. This state is characterized by the fact that a large number of indistinguishable bosons occupy the ground state. It took about 70 years until an experimental realization of the Bose-Einstein condensation in ultracold dilute alkali-metal gases was achieved in 1995 [3, 4]. This was a major break-through and opened the gates to an exciting new field of research, both experimentally and theoretically. In dilute gases, the correlations between atoms are weak and unlike in the theory of superfluid liquid ^{4}He, a mean-field theoretical approach can be applied. Therefore these systems can be described by a macroscopic condensate wave function $\psi(\mathbf{r}, t)$ that characterizes the static and dynamical behaviour of the Bose-Einstein condensate (BEC). This wave function obeys a nonlinear Schrödinger equation known as the Gross-Pitaevskii equation [5, 6].

The research of vortices in classical fluids has a very long history. When Leonardo da Vinci drew his famous sketches of water turbulence in the 16th century, he realized that turbulence consists of many eddies of different sizes. It was in 1858 that Helmholtz proposed the idea of a vortex filament [7]. The most important difference between the physics of the vortices in quantum systems and those in classical systems, is the quantized circulation which is due to the single-valuedness of the condensate wave function. The first experimental detection of a vortex in an atomic BEC was made by Matthews *et al.* in 1999 [8]. Soon afterwards, vortex creation in BECs was reported by several groups using a range of different techniques [9, 10, 11]. Related highly active fields of research are the study of vortices in two-component Bose-Einstein condensates, the study of vortices in condensates with dipolar interaction [12] and the investigation of the dynamics and stability properties of a single off-axis vortex [13].

A common experimental method to create vortices in BECs is to confine the atoms in a static, cylindrically symmetric magnetic trap, upon which a nonaxisymmetric dipole potential is superimposed, created by a stirring laser beam. The gas is evaporatively cooled to Bose-Einstein condensation, while the superimposed laser potential is rotated with angular frequency Ω (see Figure 1). Intuitively, this scheme refers to stirring the condensate

Figure 1 – A cigar-shaped condensate is confined by an axisymmetric magnetic trap and stirred by an off-center far-detuned laser beam. The laser beam propagates along the long axis and creates an anisotropic quadrupole potential that rotates at an angular velocity Ω. The image is taken from Ref. [14].

mechanically and is analogous to the seminal "rotating bucket" experiment in classical hydrodynamics [15]. In Figure 2 images taken during an experiment by Madison *et al.* using this technique are displayed. Since the vortex core radius is too small for direct visualization, a time of flight method was used to obtain the images, where the trap is turned off, allowing the condensate to expand. The initial tight radial confinement means that this expansion is mostly in the radial direction, and the expanded condensate usually becomes disc-shaped. The vortices are clearly visible as dark spots in the otherwise bright density profile of the trapped BEC.

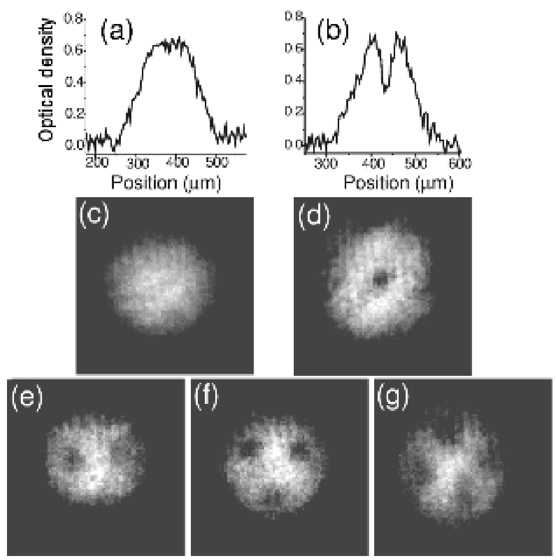

Figure 2 – Absorption images of a BEC stirred with a laser beam. In all images the condensate consists of about 1.4×10^5 atoms, the temperature is below 80 nK and the rotation rate $\Omega/2\pi$ increases from 145 Hz for (a) and (c) to 168 Hz for (g). Images (a) and (b) show the optical thickness for images (c) and (d), with the clear appearance of the vortex core. Images (e), (f), and (g) show states with two, three, and four vortices. The pictures are taken from Ref. [14].

In this work, we study the static and dynamic properties of a single vortex in a one-component Bose-Einstein condensate. In Section 2 we introduce the Gross-Pitaevski equation and the Thomas-Fermi limit and show that the circulation of a vortex in a BEC is quantized. In Section 3 we derive within a variational approach approximate equations of motion for a condensate with a centered vortex and discuss equilibrium points. Furthermore we calculate the energies for a condensate with and without a vortex and obtain the critical rotation frequency for a rotating trap at which a vortex state becomes stable. We then investigate the behavior of the condensate in free expansion after the trapping potential is turned off. Finally in Section 4 we review what we have achieved and discuss possible continuations of our research work.

2 Gross-Pitaevskii Equation

The dynamics of a Bose-Einstein condensate at zero temperature is determined by the time-dependent Gross-Pitaevskii (GP) equation [5, 6]

$$i\hbar\frac{\partial\psi(\mathbf{r},t)}{\partial t} = \left[-\frac{\hbar^2}{2M}\nabla^2 + V(\mathbf{r}) + g|\psi(\mathbf{r},t)|^2\right]\psi(\mathbf{r},t). \tag{1}$$

In general $V(\mathbf{r})$ is an arbitrary external potential. In this work, we specialize on a cylindrical trap potential

$$V(\rho,z) = \frac{M}{2}\omega_\rho^2(\rho^2+\gamma^2 z^2), \tag{2}$$

which will be the reference point for the following calculations. Here $\gamma = \frac{\omega_z}{\omega_\rho}$ is the ratio of the trap frequencies. The two-particle interaction strength g is given by

$$g = \frac{4\pi\hbar^2 a_s}{M}, \tag{3}$$

where, as we are in the low-energy limit, only the s-wave scattering is important and a_s denotes the s-wave scattering length [16]. Note that only two-particle interactions are considered, which is an appropriate approximation for dilute gases. The GP equation is often referred to as a nonlinear Schrödinger equation where the nonlinearity arises from the two-particle interaction and the wavefunction is normalized to the particle number N, which leads to the normalization condition

$$N = \int |\psi(\mathbf{r},t)|^2 d^3r. \tag{4}$$

Performing the following ansatz for a separation of time

$$\psi(\mathbf{r},t) = \psi(\mathbf{r})\,\mathrm{e}^{-\frac{i}{\hbar}\mu t} \tag{5}$$

and inserting it into equation (1) we arrive at the time-independent GP-equation

$$\mu\psi(\mathbf{r}) = \left[-\frac{\hbar^2}{2M}\nabla^2 + V(\mathbf{r}) + g|\psi(\mathbf{r})|^2\right]\psi(\mathbf{r}). \tag{6}$$

Here μ represents the chemical potential, which is determined by the normalization condition (4).

2.1 Thomas-Fermi Approximation

We now consider the stationary case without a vortex. For large clouds with a large number of particles an accurate approximation to the ground-state wave function may be obtained by neglecting the kinetic energy term in equation (6), which then simplifies to

$$n(\mathbf{r}) = |\psi(\mathbf{r})|^2 = \frac{\mu - V(\mathbf{r})}{g}, \tag{7}$$

and $n(\mathbf{r}) = 0$, if the right-hand side becomes negative. Here the boundaries of the cloud are determined by the condition

$$V(\mathbf{r}) = \mu. \tag{8}$$

This leads to the so-called Thomas-Fermi (TF) radii which give the extension in radial and axial direction of the cloud

$$R_\perp = \sqrt{\frac{2\mu}{M w_\rho^2}}, \quad R_\| = \sqrt{\frac{2\mu}{M(w_\rho \gamma)^2}}. \tag{9}$$

The chemical potential μ has to be calculated using the normalization condition (4) and in case of the trap potential (2) turns out to be:

$$\mu = \left[\frac{15 w_\rho^3 \gamma N g}{8\pi} \left(\frac{M}{2}\right)^{\frac{3}{2}}\right]^{\frac{2}{5}}. \tag{10}$$

Finally the density profile has a parabolic shape

$$n_{\mathrm{TF}}(\rho, z) = n_{\mathrm{TF0}} \left[1 - \left(\frac{\rho}{R_\perp}\right)^2 - \left(\frac{z}{R_\|}\right)^2\right], \tag{11}$$

where the density at the trap center is given by

$$n_{\mathrm{TF0}} = \frac{\mu}{g}. \tag{12}$$

2.2 Superfluid Velocity and Quantized Circulation

Multiplying the time-dependent GP equation (1) with $\psi^*(\mathbf{r}, t)$ and substracting its complex conjugate, one arrives at:

$$\frac{\partial |\psi|^2}{\partial t} + \nabla \left[\frac{\hbar}{2Mi}(\psi^* \nabla \psi - \psi \nabla \psi^*)\right] = 0, \tag{13}$$

which has the form of a continuity equation for the particle density n and may be written as

$$\frac{\partial n}{\partial t} + \nabla(n\mathbf{v}) = 0, \tag{14}$$

where the velocity $\mathbf{v}$ of the condensate is defined by

$$\mathbf{v} = \frac{\hbar}{2Mi} \frac{(\psi^* \nabla \psi - \psi \nabla \psi^*)}{|\psi|^2}. \tag{15}$$

Using the Madelung transformation [17] the condensate wave function can be written in terms of its density $n = |\psi|^2$ and phase $S(\mathbf{r}, t)$ by

$$\psi = \sqrt{n}\, \mathrm{e}^{iS}. \tag{16}$$

Inserting equation (16) into equation (15) reveals a simple expression for the condensate velocity which depends on the gradient of the phase

$$\mathbf{v} = \frac{\hbar}{M}\nabla S. \tag{17}$$

This has far-reaching consequences for the possible motion of the condensate, since it immediately follows, that

$$\nabla \times \mathbf{v} = 0 \tag{18}$$

and, therefore, the velocity field is irrotational unless the phase shows a singularity.
From the single-valuedness of the condensate wave function it follows that, around a closed loop C, the change in phase ΔS must be an integer multiple of 2π. Thus the circulation κ which is defined by

$$\kappa = \oint_C \mathbf{v} d\mathbf{r}, \tag{19}$$

is calculated to be

$$\kappa = 2\pi l \frac{\hbar}{M}, \tag{20}$$

where l is an integer number. This result reveals, as was first proposed by Onsager [18] in the context of superfluid liquid ^{4}He, that the circulation is quantized. For a vortex line at ρ_0 equation (18) generalizes under consideration of (20) to

$$\nabla \times \mathbf{v} = 2\pi l \frac{\hbar}{M} \delta^{(2)}(\boldsymbol{\rho} - \boldsymbol{\rho_0})\hat{\mathbf{z}}, \tag{21}$$

where $\delta^{(2)}$ is the two-dimensional Dirac delta function and $\boldsymbol{\rho}$ the polar vector in the xy plane.

3 Variational Approach

In this section we use a variational approach to obtain approximate equations of motions for parameters of a suitable trial function. This technique is well-established and has been successfully applied in several previous studies [19, 20].

3.1 Least Action Principle

Multiplying the time-dependent GP equation (1) with $\delta\psi^*$ and its complex conjugate with $\delta\psi$ and integrating over space and time, we are led to the equivalent least action principle:

$$\delta\mathcal{A}[\psi^*, \psi] = 0, \tag{22}$$

with the action

$$\mathcal{A} = \int dt \int d^3r \mathcal{L} \tag{23}$$

and the Lagrange density

$$\begin{aligned}\mathcal{L} =& \frac{i\hbar}{2}\left[\psi^*(\mathbf{r},t)\frac{\partial\psi(\mathbf{r},t)}{\partial t} - \psi(\mathbf{r},t)\frac{\partial\psi^*(\mathbf{r},t)}{\partial t}\right] - \frac{\hbar^2}{2M}\nabla\psi(\mathbf{r},t)\nabla\psi^*(\mathbf{r},t) \\ & - V(\mathbf{r})\psi(\mathbf{r},t)\psi^*(\mathbf{r},t) - \frac{1}{2}g\psi^*(\mathbf{r},t)^2\psi(\mathbf{r},t)^2.\end{aligned} \tag{24}$$

Inserting a suitable trial function with time-dependent parameters into equation (24) and integrating over space, leads to the Lagrange function

$$L = \int d^3r\mathcal{L} \tag{25}$$

of the system. With the help of the Euler-Lagrange formalism

$$\frac{\mathrm{d}}{\mathrm{d}t}\frac{\partial L}{\partial \dot{q}_i} - \frac{\partial L}{\partial q_i} = 0 \tag{26}$$

we arrive at effective Lagrangian equations of motion for our time-dependent variational parameters q_i. Although not exact, this method gives a good qualitative and quantitative description of the underlying physical problem.

3.2 Finding a Suitable Trial Function

We now consider a Bose-Einstein condensate with a vortex in the harmonic trap with cylindrical symmetry from equation (2). In this case, the phase S only depends on the polar angle φ and equation (16) transforms to

$$\psi(\rho,z,\varphi) = \sqrt{n(\rho,z)}\,\mathrm{e}^{il\varphi} = f(\rho,z)\,\mathrm{e}^{il\varphi}\,. \tag{27}$$

Inserting equations (2) and (27) into (6) leads to an equation for the amplitude f:

$$-\frac{\hbar^2}{2M}\left[\frac{1}{\rho}\frac{\partial}{\partial\rho}\left(\rho\frac{\partial f}{\partial\rho}\right) + \frac{\partial^2 f}{\partial z^2}\right] + \frac{\hbar^2}{2M\rho^2}l^2 f + \frac{M}{2}\omega_\rho^2(\rho^2+\gamma^2 z^2)f + gf^3 = \mu f. \tag{28}$$

As we can see, the superflow term containing the angular momentum l represents a centrifugal barrier proportional to $1/\rho^2$. Thus the amplitude has to vanish at $\rho = 0$, as otherwise the equation collapses. To determine the length scale ζ of the vortex core size, we compare the relevant energies near the trap center which are the kinetic energy that is proportional to $\hbar^2/2M\zeta^2$, and the interaction energy, which is proportional to $f^2 g$. For the amplitude to return to its bulk value these energies must approximately be the same and the resulting length scale is determined to be

$$\zeta = \sqrt{\frac{\hbar^2}{2Mgf^2(\zeta,0)}} = \frac{1}{\sqrt{8\pi a f^2(\zeta,0)}}. \tag{29}$$

Here $f^2(\zeta, 0)$ is taken to be the local Thomas-Fermi density without a vortex at the trap-center n_{TF0} and ζ is called the coherence length. Combining equations (9), (12) and (29) we are led to the important relation

$$\frac{\zeta}{d_{\mathrm{ho}}} = \frac{d_{\mathrm{ho}}}{R_\perp}, \quad d_{\mathrm{ho}} = \sqrt{\frac{\hbar}{M\omega_\rho}}. \tag{30}$$

The TF oscillator length d_{ho} is the geometric mean of ζ and $R_\perp$, and equation (30) then yields a clear separation of TF length scales $\zeta \ll d_{\mathrm{ho}} \ll R_\perp$.

We now obtain approximate solutions of equation (28) for the amplitude f in the cases $\rho \ll \zeta$ and $\zeta \ll \rho < R_\rho$ respectively, where R_ρ is the radial extension of the cloud. For $\rho \ll \zeta$ the dominant terms in equation (28) arise from the kinetic energy and the associated derivatives with respect to ρ. Thus we neglect all other terms and are left with

$$-\frac{\hbar^2}{2M}\left[\frac{1}{\rho}\frac{\partial}{\partial\rho}\left(\rho\frac{\partial f}{\partial\rho}\right)\right] + \frac{\hbar^2}{2M\rho^2}l^2 f = 0. \tag{31}$$

Solving for f yields the ρ-dependence

$$f = c\rho^l, \quad n = c^2\rho^{2l}, \quad \rho \ll \zeta, \tag{32}$$

where c is a suitable constant. On the other hand, for $\zeta \ll \rho < R_\rho$, the kinetic energy can be neglected and we are left with the familiar Thomas-Fermi solution (11).
A suitable trial function for a variational approach has to reconcile both asymptotic forms (11) and (32), which is done by the following function

$$\psi(\rho, z, \varphi) = C\sqrt{\left(\frac{\rho^2}{\rho^2+\xi^2}\right)^l\left[1-\left(\frac{\rho}{R_\rho}\right)^2-\left(\frac{z}{R_z}\right)^2\right]}\,\mathrm{e}^{il\varphi}\,. \tag{33}$$

Here ξ specifies the distance at which the condensate density reaches half of the value of a condensate without a vortex at the trap center and hence characterizes the size of the vortex core. This value is supposed to be of the order of the coherence length ζ introduced in (29) and, therefore, should be small compared to the other relevant quantities. The exponential term on the right-hand side is essential for the wavefunction of a rotating Bose-Einstein condensate, since the phase is responsible for the angular velocity as discussed in Section 2.2. In general it costs energy to create a vortex and the amount of this energy is dominated by the kinetic energy of the superfluid flow due to the vortex. In the case of a cylindrically symmetric trap it follows from equations (20) and (27) that the velocity is given by

$$v_\varphi = \frac{l\hbar}{M\rho}. \tag{34}$$

Thus the energy associated with the superfluid flow is of the order of

$$E_{\mathrm{v}} = \int d^3r\frac{1}{2}Mn\mathbf{v}^2 = \frac{l^2\hbar^2}{2M}\int d^3r\frac{n}{\rho^2}. \tag{35}$$

We see that E_{v} increases with l^2 and therefore it is energetically favorable for higher quantized vortices to decay into multiple singly quantized vortices. Here E_{v} stands for the leading term in the energy it costs to create a vortex. Hence, the most important case is $l = 1$, and so we will restrict ourselves from now on to the study of this particular case.

3.3 Obtaining the Lagrange Function

Taking (33) as a reference point, we choose our time-dependent trial function to be of the following form

$$\psi(\rho, z, \varphi, t) = C(t)\sqrt{\frac{\rho^2}{\rho^2 + R_\rho(t)^2\beta(t)^2}\left\{1 - \left[\frac{\rho}{R_\rho(t)}\right]^2 - \left[\frac{z}{R_z(t)}\right]^2\right\}}\, \mathrm{e}^{i\varphi + iB_\rho(t)\rho^2 + iB_z(t)z^2}\,. \tag{36}$$

Here $R_z(t)$, $R_\rho(t)$, $\beta(t)$, $B_\rho(t)$ and $B_z(t)$ are time-dependent variational parameters, where $B_\rho(t)$ and $B_z(t)$ are necessarily included to describe the condensate dynamics. Note, that we have introduced $\beta(t) = \xi(t)/R_\rho(t)$ which is the ratio of the vortex core size to the radial extension of the cloud. Furthermore, we have set the angular momentum quantum number l to 1, since, as has been shown in Subsection 3.2, higher quantized vortices decay into multiple singly quantizes vortices. Inserting (36) into the Lagrange density from equation (24), the Lagrange function is obtained by integrating over space. The condensate density has to remain positive, which gives a condition for the integration domain for z and ρ:

$$1 - \left[\frac{\rho}{R_\rho(t)}\right]^2 - \left[\frac{z}{R_z(t)}\right]^2 \geq 0. \tag{37}$$

For reasons of lucidity we introduce the following abbreviation

$$A_1(t) = \sqrt{1 + \beta(t)^2}\,\mathrm{Arcsch}[\beta(t)] \tag{38}$$

and

$$A_2(t) = -3 + 5\beta(t)^2\left[3A_1 - 4 + 3\beta(t)^2\left(A_1 - 1\right)\right]. \tag{39}$$

The normalization constant $C(t)$ in (36) is determined via the normalization condition (4) and turns out to be

$$C(t) = \sqrt{-\frac{45N}{8\pi R_\rho(t)^2 R_z(t) A_2(t)}}. \tag{40}$$

The Lagrange function can be split into four parts which are now to be calculated separately:

$$L = L_{\mathrm{time}} + L_{\mathrm{kin}} + L_{\mathrm{pot}} + L_{\mathrm{int}}. \tag{41}$$

The potential part

$$L_{\mathrm{pot}} = -\int d^3r V(\mathbf{r})|\psi(\mathbf{r}, t)|^2 \tag{42}$$

gives

$$L_{\rm pot} = -MN\omega_\rho^2 \left[-\frac{3}{7}\frac{R_\rho(t)^2}{A_2(t)} - \frac{\beta(t)^2 R_\rho(t)^2}{2} + \frac{\gamma^2 R_z(t)^2(1+\beta(t)^2)}{10} + \frac{6\gamma^2 R_z(t)^2}{70A_2(t)} \right]. \tag{43}$$

The part arising from the interaction

$$L_{\rm int} = -\frac{g}{2}\int d^3r|\psi(\mathbf{r},t)|^4 \tag{44}$$

is calculated to be

$$L_{\rm int} = \frac{9N^2 g}{\pi R_\rho(t)^2 R_z(t)} \left[\frac{9\beta(t)^2}{8A_2(t)} + \frac{1}{2A_2(t)} + \frac{27}{28A_2(t)^2} \right]. \tag{45}$$

The part denoted with $L_{\rm time}$ is

$$L_{\rm time} = \frac{i\hbar}{2}\int d^3r \left[\psi^*(\mathbf{r},t)\frac{\partial\psi(\mathbf{r},t)}{\partial t} - \psi(\mathbf{r},t)\frac{\partial\psi^*(\mathbf{r},t)}{\partial t} \right] \tag{46}$$

and gives

$$L_{\rm time} = \hbar N \left\{ \frac{6R_z(t)^2\dot{B}_z(t)}{35A_2(t)} + \frac{[1+\beta(t)^2]R_z(t)^2\dot{B}_z(t)}{5} - \frac{6R_\rho(t)^2\dot{B}_\rho(t)}{7A_2(t)} - R_\rho(t)^2\dot{B}_\rho(t)\beta(t)^2 \right\}. \tag{47}$$

The kinetic contribution is

$$L_{\rm kin} = -\frac{\hbar^2}{2M}\int d^3r \nabla\psi(\mathbf{r},t)\nabla\psi^*(\mathbf{r},t). \tag{48}$$

Remembering that the Thomas-Fermi approximation corresponds to neglecting the kinetic energy part arising from the curvature of the slowly varying condensate background envelope $\sqrt{1-[\rho/R_\rho(t)]^2-[z/R_z(t)]^2}$, we follow Ref. [12] and drop all terms that are due to the gradient of this part. The kinetic contribution to the Lagrange function is thus calculated in TF approximation to be

$$\begin{aligned} L_{\rm kin} =& \frac{N\hbar^2}{m}\Bigg(-\frac{65}{8R_\rho(t)^2 A_2(t)} - \frac{165\beta(t)^2}{16R_\rho(t)^2 A_2(t)} \\ &+ \frac{12R_\rho(t)^2B_\rho(t)^2}{7A_2(t)} - \frac{6R_\rho(t)^2B_\rho(t)^2\beta(t)^2}{A_2(t)} - \frac{40R_\rho(t)^2B_\rho(t)^2\beta(t)^4}{A_2(t)} - \frac{30R_\rho(t)^2B_\rho(t)^2\beta(t)^6}{A_2(t)} \\ &+ \frac{6R_z(t)^2B_z(t)^2}{7A_2(t)} + \frac{46R_z(t)^2B_z(t)^2\beta(t)^2}{5A_2(t)} + \frac{14R_z(t)^2B_z(t)^2\beta(t)^4}{A_2(t)} + \frac{6R_z(t)^2B_z(t)^2\beta(t)^6}{A_2(t)} \\ &+ \frac{3A_1(t)}{16A_2(t)}\Bigg\{ \frac{40+80\beta(t)^2+55\beta(t)^4}{[1+\beta(t)^2]R_\rho(t)^2} + 160\beta(t)^4[1+\beta(t)^2]R_\rho(t)^2B_\rho(t)^2 \\ &+32\beta(t)^2[1+\beta(t)^2]^2R_z(t)^2B_z(t)^2\Bigg\}\Bigg). \end{aligned} \tag{49}$$

Since $\beta(t)$ is small, we neglect from now on all terms of higher than second order in β. After introducing the following abbreviations

$$A_3(t) = \beta(t)^2 \left\{ 30 \ln \left[\frac{2}{\beta(t)} \right] - 61 \right\}, \tag{50}$$

$$A_4(t) = 30 + \beta(t)^2 \left\{ 349 - 120 \ln \left[\frac{2}{\beta(t)} \right] \right\}, \tag{51}$$

$$A_5(t) = 4\hbar^2 B_z(t)^2 + M[M\omega_\rho^2\gamma^2 - 2\hbar\dot{B}_z(t)], \tag{52}$$

$$A_6(t) = 4\hbar^2 B_\rho(t)^2 + M[M\omega_\rho^2 - 2\hbar\dot{B}_\rho(t)], \tag{53}$$

$$A_7(t) = 38 - 15 \ln \left[\frac{2}{\beta(t)} \right], \tag{54}$$

$$A_8(t) = 410 + 3 \ln \left[\frac{2}{\beta(t)} \right] \left\{ -187 + 60 \ln \left[\frac{2}{\beta(t)} \right] \right\}, \tag{55}$$

$$A_9(t) = \left[-78 + 72 \ln \left[\frac{2}{\beta(t)} \right] + \beta(t)^2 \left\{ 439 + 360 \ln \left[\frac{2}{\beta(t)} \right]^2 - 762, \ln \left[\frac{2}{\beta(t)} \right] \right\} \right] \tag{56}$$

the Lagrange function becomes

$$L = -\frac{NgA_4(t)}{56\pi R_\rho(t)^2 R_z(t)} - \frac{5\hbar^2 A_9(t)}{144 M R_\rho(t)^2} - \frac{A_6(t) R_\rho(t)^2 \left[6 + A_3(t)\right]}{42} + \frac{A_5(t) R_z(t)^2 \left[-15 + A_3(t)\right]}{210}. \tag{57}$$

3.4 Equations of Motion

Now that we have obtained the Lagrange function of the system, we proceed by minimizing the corresponding action with respect to our variational parameters. This leads to Euler-Lagrange equations of the form (26). Minimizing for $R_\rho(t)$ gives

$$\begin{aligned} &18NgA_4(t) + \frac{35\pi\hbar^2 A_9(t) R_z(t)}{M} \\ &- 48\pi \left[6 + A_3(t)\right] R_\rho(t)^4 R_z(t) \left[\frac{2\hbar^2}{M} B_\rho(t)^2 + \frac{1}{2} M\omega_\rho^2 - \hbar\dot{B}_\rho(t) \right] = 0. \end{aligned} \tag{58}$$

Minimizing with respect to $R_z(t)$ yields

$$15NgA_4(t) - 16\pi R_\rho(t)^2 R_z(t)^3 \left[15 - A_3(t)\right] \left[\frac{2\hbar^2}{M} B_z(t)^2 + \frac{1}{2} M\omega_\rho^2\gamma^2 - \hbar\dot{B}_z(t) \right] = 0. \tag{59}$$

Varying $\beta(t)$, we get

$$\begin{aligned}45MNg\left\{-409+120\ln\left[\frac{2}{\beta(t)}\right]\right\}\beta(t)^2-175\pi\hbar^2A_8(t)R_z(t)\beta(t)^2+3150\hbar^2\pi R_z(t)\\+48\pi MR_\rho(t)^2R_z(t)\beta(t)^2A_7(t)\left\{5R_\rho(t)^2\left[\frac{2\hbar^2}{M}B_\rho(t)^2+\frac{1}{2}M\omega_\rho^2-\hbar\dot{B}_\rho(t)\right]\right.\\\left.-R_z(t)^2\left[\frac{2\hbar^2}{M}B_z(t)^2+\frac{1}{2}M\omega_\rho^2\gamma^2-\hbar\dot{B}_z(t)\right]\right\}=0.\end{aligned} \tag{60}$$

Finally, minimizing for $B_\rho(t)$ and $B_z(t)$ we obtain

$$B_\rho(t)=\frac{M}{2\hbar}\left[\frac{2\beta(t)A_7(t)\dot{\beta}(t)}{6+A_3(t)}-\frac{\dot{R}_\rho(t)}{R_\rho(t)}\right] \tag{61}$$

and

$$B_z(t)=\frac{M}{2\hbar}\left[\frac{2\beta(t)A_7(t)\dot{\beta}(t)}{-15+A_3(t)}-\frac{\dot{R}_z(t)}{R_z(t)}\right]. \tag{62}$$

Inserting (61) and (62) into (58)–(60) and rescaling to dimensionless variables

$$r_\rho=R_\rho/\sqrt{\frac{\hbar}{M\omega_\rho}},\quad r_z=R_z/\sqrt{\frac{\hbar}{M\omega_\rho}},\quad \tau=\omega_\rho t,\quad P=\frac{MN}{4\pi\hbar^2}/\sqrt{\frac{\hbar}{M\omega_\rho}}g, \tag{63}$$

we arrive at a system of three coupled ordinary differential equations. We again expand up to second order in β and after rearranging the equations we are led to

$$\begin{aligned}\ddot{r}_z(\tau) =& -\frac{15PA_4(\tau)}{2(A_3(\tau)-15)r_\rho(\tau)^2r_z(\tau)^2} + \frac{4\beta(\tau)A_7(\tau)\dot{r}_z(\tau)\dot{\beta}(\tau)}{A_3(\tau)-15} \\ &+ \frac{2\left(15+A_7(\tau)\right)r_z(\tau)\dot{\beta}(\tau)^2}{A_3(\tau)-15} - \frac{4\beta(\tau)^2A_7(\tau)^2r_z(\tau)\dot{\beta}(\tau)^2}{15\left[A_3(\tau)-15\right]} \\ &- \gamma^2r_z(\tau) + \frac{2\beta(\tau)A_7(\tau)r_z(\tau)\ddot{\beta}(\tau)}{A_3(\tau)-15},\end{aligned} \tag{64}$$

$$\begin{aligned}\ddot{r}_\rho(\tau) =& \frac{35A_9(\tau)}{24[6+A_3(\tau)]r_\rho(\tau)^3} \\ &+ \frac{3A_4(\tau)P}{[6+A_3(\tau)]r_\rho(\tau)^3r_z(\tau)} - r_\rho(\tau) + \frac{2A_7(\tau)^2\beta(\tau)^2r_\rho(\tau)^2\dot{\beta}(\tau)^2}{3[6+A_3(\tau)]} \\ &+ \frac{2[15+A_7(\tau)]r_\rho(\tau)\dot{\beta}(\tau)^2}{6+A_3(\tau)} + \frac{2A_7(\tau)\beta(\tau)[2\dot{r}_\rho(\tau)\dot{\beta}(\tau)+r_\rho(\tau)\ddot{\beta}(\tau)]}{6+A_3(\tau)},\end{aligned} \tag{65}$$

$$\begin{aligned}\ddot{\beta}(\tau) =& \left(\frac{7875}{4A_7(\tau)\beta(\tau)^2r_\rho(\tau)^2} - r_z(\tau)\left[15\ddot{r}_z(\tau) + 4A_7(\tau)\beta(\tau)\dot{\beta}(\tau)\dot{r}_z(\tau)\right] - \frac{875A_8(\tau)}{8A_7(\tau)r_\rho(\tau)^2}\right. \\ &+15\left[5r_\rho(\tau)^2 - \gamma^2r_z(\tau)^2\right] + 25r_\rho(\tau)\left[3\ddot{r}_\rho(\tau) - 2A_7(\tau)\beta(\tau)\dot{\beta}(\tau)\dot{r}_\rho(\tau)\right] \\ &+\left.\frac{225P\left\{-409+120\ln\left[2/\beta(t)\right]\right\}}{2A_7(\tau)r_z(\tau)r_\rho(\tau)^2}\right)/A_7(\tau)\beta(\tau)\left[25r_\rho(\tau)^2+2r_z(\tau)^2\right].\end{aligned} \tag{66}$$

Notice that the resulting dynamics is essentially due to having introduced the variational parameters $B_\rho(t)$ and $B_z(t)$ in the ansatz (36).

3.5 Equilibrium Positions

We now study the stationary points of the system and therefore set all velocities and accelerations to zero. This reduces equations (64)–(66) to

$$\gamma^2r_{z0} = -\frac{15PA_4}{2(A_3-15)r_{\rho0}^2r_{z0}^2}, \tag{67}$$

$$r_{\rho0} = \frac{35A_9}{24[6+A_3]r_{\rho0}^3} + \frac{3A_4P}{[6+A_3]r_{\rho0}^3r_{z0}}, \tag{68}$$

$$15\gamma^2r_{z0}^2 = \frac{7875}{4A_7\beta_0^2r_{\rho0}^2} + \frac{225P\left\{-409+120\ln\left[\frac{2}{\beta_0}\right]\right\}}{2A_7r_{z0}r_{\rho0}^2} + 75r_{\rho0}^2 - \frac{875A_8}{8A_7r_{\rho0}^2}. \tag{69}$$

3.5.1 Approximate Analytical Solution

Apart from a numerical solution of these equations, we are also interested in an approximate analytical expression for the equilibrium positions. Therefore we solve equation (67) for P

and neglect the part that goes with β^2, which gives

$$P = \frac{1}{15}\gamma^2 r_{\rho 0}^2 r_{z0}^3. \tag{70}$$

Inserting this result into equations (68) and (69), and again only taking terms in β to lowest order with us, we are led to

$$r_{z0}^2 = \frac{455}{24\gamma^2 r_{\rho 0}^2} - \frac{10\ln\left[\frac{2}{\beta_0}\right]}{\gamma^2 r_{\rho 0}^2} + \frac{r_{\rho 0}^2}{\gamma^2} \tag{71}$$

and

$$105 = \beta_0^2\left[\frac{35}{6}A_8 - 4A_7 r_{\rho 0} - 12\gamma^2\left(-97 + 30\ln\left[\frac{2}{\beta_0}\right]\right) r_{\rho 0}^2 r_{z0}^2\right]. \tag{72}$$

Eliminating r_{z0} between equations (71) and (72) we obtain an equation depending on β_0 and $r_{\rho 0}$. Solving for $r_{\rho 0}$ only one positive, real solution exists, namely

$$r_{\rho 0} = \frac{5^{1/4}\left(36 - \beta_0^2\left\{2081 - 2676\ln\left[\frac{2}{\beta_0}\right] + 720\ln\left[\frac{2}{\beta_0}\right]^2\right\}\right)^{1/4}}{2^{3/4}\sqrt{3\beta_0}}. \tag{73}$$

Neglecting the terms in the bracket on the right-hand side that go with β_0^2 and solving for β_0 we obtain

$$\beta_0 = \frac{\sqrt{\frac{5}{2}}}{r_{\rho_0}^2}. \tag{74}$$

This result is consistent with other studies [21] and coincides up to a factor of $\sqrt{5/2}$ with the coherence length of equation (30) which certifies that the length scale of the vortex core size is indeed determined by the coherence length. Solving (74) for $r_{\rho 0}$, inserting the result into equation (71) and neglecting terms of higher order in β_0 leads to the analogous approximate dependence of β_0 on r_{z0}

$$\beta_0 = \frac{\sqrt{\frac{5}{2}}}{\gamma^2 r_{z0}^2}. \tag{75}$$

Reintroducing the rescaled scattering length P from equation (70) we arrive at approximate equations for the fixpoint positions of the condensate

$$\beta_0 = \frac{5^{1/10}}{\sqrt{2}(3P\gamma)^{2/5}}, \tag{76}$$

$$r_{\rho 0} = (15P\gamma)^{1/5}, \tag{77}$$

$$r_{z0} = \frac{r_{\rho 0}}{\gamma}. \tag{78}$$

Note that equations (77) and (78) coincide with the TF-Radii $R_\perp$ and $R_\parallel$ from equation (9) and (10) for a condensate without a vortex in our rescaled units. This proves that the spatial extension of the condensate is not significantly influenced by the presence of a vortex.
However, we are also interested in the first corrections to (77) and (78) in order to see in which direction the radii are altered due to the presence of a vortex. Therefore, we insert the approximate solution for β_0 into the fixpoint equations (67) and (68) and replace $r_{\rho 0} \to r_{\rho-\mathrm{TF}} + \delta r_\rho$ and $r_{z0} \to r_{z-\mathrm{TF}} + \delta r_z$ where $r_{\rho-\mathrm{TF}}$ and $r_{z-\mathrm{TF}}$ are the approximate solutions from equations (77) and (78). Since the corrections δr_ρ and δr_z are supposed to be small, we only take first order terms with us and solve the resultant system of two linear equations in δr_ρ and δr_z. The leading terms are straightforwardly determined to be

$$\begin{aligned}
\delta r_\rho = & \left\{-24.59 + 845.43 P\gamma + 414.16 (P\gamma)^{1/5} \right. \\
& -2\left[24.66 + 22.69 P\gamma - 289.90 (P\gamma)^{1/5}\right] \ln(P\gamma) + 4\left[-3.18 + 8.42 (P\gamma)^{1/5}\right] \ln^2(P\gamma) \left.\right\} \\
& / \left[24.0 (P\gamma)^{4/5} + 3.39 P\gamma + 5.78 P\gamma \ln(P\gamma)\right]^2 , \qquad (79) \\
\delta r_z = & \left\{16.39 - 97.55 P\gamma - 166.35 (P\gamma)^{1/5} \right. \\
& + \left[6.42 - 45.38 P\gamma + 26.28 (P\gamma)^{1/5}\right] \ln(P\gamma) + 4\left[2.13 - 13.19 (P\gamma)^{1/5}\right] \ln^2(P\gamma) \left.\right\} \\
& / \left\{\gamma \left[24.0 (P\gamma)^{4/5} + 3.39 P\gamma + 5.78 P\gamma \ln(P\gamma)\right]^2 \right\} . \qquad (80)
\end{aligned}$$

We see that for reasonable values of P and γ with $P\gamma \gg 1$, δr_ρ is positive and δr_z is negative. Thus the vortex pushes the condensate apart in radial direction, letting in shrink slightly in the z-direction.

3.5.2 Numerical Solution

The exact fixpoint equations (67)–(69) cannot be solved analytically because the quantities are correlated in an essentially non-algebraic way. Therefore we solve (67)–(69) numerically for two different aspect ratios $\gamma = 5$ and $\gamma = 0.2$. In order to bring out the dependence of the various quantities upon the strength of the interaction, we plot the results as a function of the s-wave scattering length a_s, since this quantity can be controlled in an experiment via Feshbach resonances [22]. In all the calculations depicted in the following figures, we have limited the minimum value of the scattering length to be $200\sqrt{\frac{\hbar}{M\omega_\rho}}/N$, because in the limit $a_s \to 0$ the approximation we made in calculating the Lagrange function, that $\beta = \xi/R_\rho$ is small, begins to break down. Also the kinetic energy part that was neglected according to the Thomas-Fermi approximation becomes more important as the interaction energy, which is proportional to a_s, decreases. The maximum value for the scattering length was set at $a_s = 5000\sqrt{\frac{\hbar}{M\omega_\rho}}/N$. The decision, where to set the lower and upper boundary for the scattering length, was guided by the limits used in previous numerical studies [12]. The graphics also include the exact solutions to the fixpoint equations that we would have obtained if we had not expanded the Lagrange function up to second order in β. These equations were not included explicitly, as they are too cumbersome to be presented.

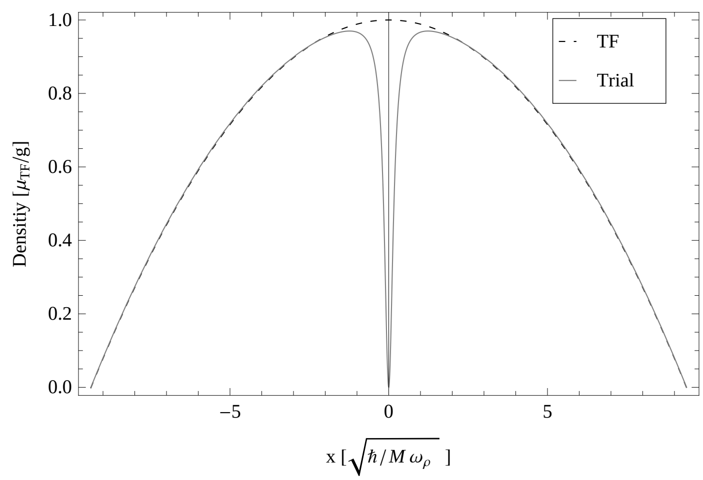

Figure 3 – Cross-section of the particle density of a BEC with a central vortex (solid curve) and without a vortex (dashed curve) at a scattering length of $a_s = 800\sqrt{\hbar/(M\omega_\rho)}/N$ at $z = y = 0$.

In Figure 3 we have displayed the cross-section of the density profile of a condensate with a vortex described by our trial function for the stationary case, where the variational parameters have been calculated numerically as pointed out in this section. We have also included the density profile of a condensate without a vortex in the Thomas-Fermi limit. The displayed density cross-sections correspond to an oblate trap ($\gamma = 5$) and to a scattering length of $a_s = 800\sqrt{\hbar/(M\omega_\rho)}/N$ at $z = y = 0$. The two profiles are very much alike, differing significantly only at the center of the trap where the vortex is located.
Figure 4 shows the radial extension of a condensate with a vortex. As the scattering length is increased, the radius widens, since the increasing repulsive interaction forces the atoms apart. Comparing the calculated radii to the TF-radii of a condensate without a vortex yields that the spatial extensions of the cloud remain nearly unaltered due to the presence of a vortex.
Figure 5 depicts the aspect ratio $\kappa = R_\rho/R_z$ of the condensate. We see that the aspect ratio equals the ratio of trap frequencies γ as it does for a condensate without a vortex. Obviously our approximation made by neglecting terms of higher than second order in β in the Lagrange function is very close to the exact value and therefore justified. Only in the case of a highly prolate trap does the radial extension become smaller and therefore the appropriateness of the expansion in $\beta = \xi/R_\rho$ begins to break down as this ratio becomes too large.
Figure 6 plots the ratio of the vortex core size to the radial size of the condensate $\beta = \xi/R_\rho$. The core radius shrinks as the scattering length is increased. Again it is the increased interaction energy that is responsible and that drives the condensate apart especially at its bulk value, which is located next to the vortex and therefore pushes against the vortex "wall".
Figure 7 plots the dependence of β on R_ρ. We see that for the oblate trap equation (74) yields an excellent result. As before, the approximation is less accurate but still fairly reasonable for a highly prolate trap.

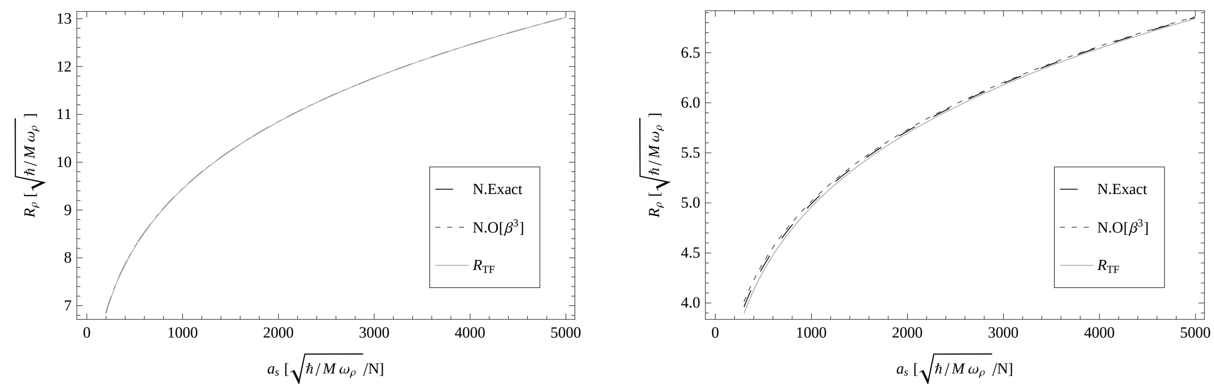

(a) $\gamma = 5$ (b) $\gamma = 0.2$

Figure 4 – The radial size R_ρ of a condensate with a vortex in an oblate trap (a) and a prolate trap (b) as a function of the scattering length a_s. Here R_ρ is measured in units of the radial harmonic oscillator length d_{ho} of the trap. Black dashed curve: Exact numerical solution. Gray dashed curve: Numerical solution for the Lagrange function expanded up to second order in β. Gray solid curve: TF-radius for a condensate without a vortex which coincides with the approximate analytical solution from equation (77) for a condensate with a vortex.

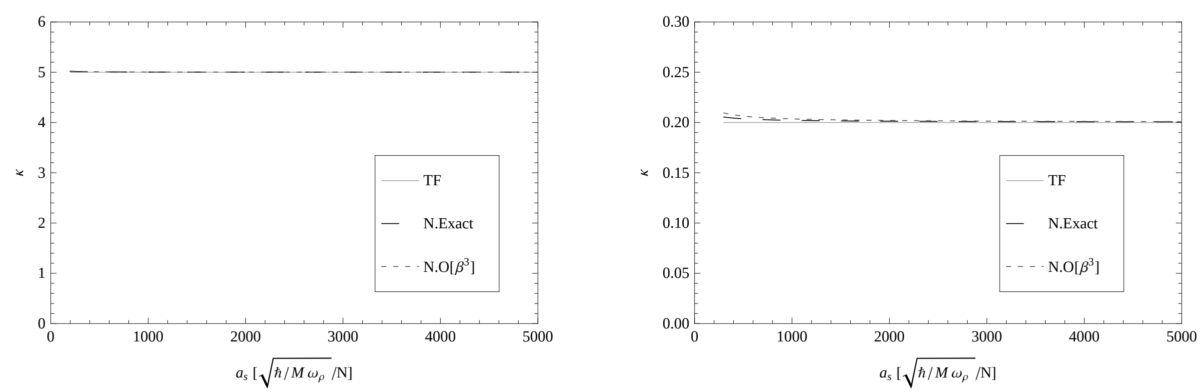

(a) $\gamma = 5$ (b) $\gamma = 0.2$

Figure 5 – The aspect ratio $\kappa = R_\rho/R_z$ of a condensate with a central vortex in an oblate trap (a) and a prolate trap (b). Black dashed curve: Exact numerical solution. Gray dashed curve: Numerical solution for the Lagrange function expanded up to second order in β. Gray solid curve: Aspect ratio of a condensate without a vortex in the TF limit.

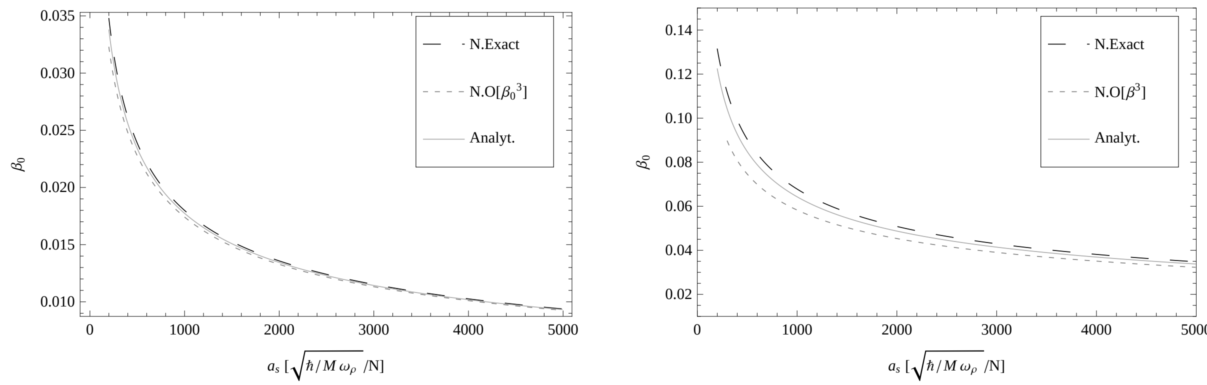

(a) $\gamma = 5$ (b) $\gamma = 0.2$

Figure 6 – The ratio of the vortex core size to radial extension $\beta = \xi/R_\rho$ of a condensate in an oblate trap (a) and in a prolate trap (b). Black dashed curve: Exact numerical solution. Gray dashed curve: Lagrange function expanded up to second order in β. Solid gray curve: Approximate analytical solution from equation (76).

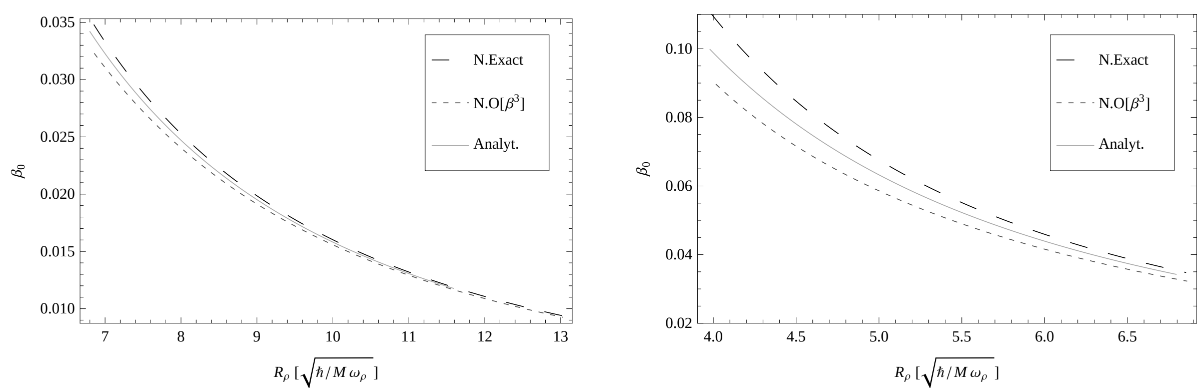

(a) $\gamma = 5$ (b) $\gamma = 0.2$

Figure 7 – Dependence of β on R_ρ for a condensate with a central vortex in an oblate trap (a) and a prolate trap (b). Black dashed curve: Exact numerical solution. Gray dashed curve: Lagrange function expanded up to second order in β. Solid gray curve: Approximate analytical solution from equation (74).

3.6 Energies and Critical Rotational Frequencies

The total energy of a condensate is the sum of the kinetic, potential and interaction energies

$$E = \frac{\hbar^2}{2M} \int d^3r \nabla\psi(\mathbf{r},t)\nabla\psi^*(\mathbf{r},t) + \int d^3r V(\mathbf{r})|\psi(\mathbf{r},t)|^2 + \frac{g}{2} \int d^3r |\psi(\mathbf{r},t)|^4. \tag{81}$$

For the stationary case, the Lagrange function reduces to the negative energy of the system and the respective integrals have already been calculated in equations (43), (45), (47) and (49). Note that all accelerations and velocities have to be set to zero, as well as the variational parameters B_ρ and B_z analogous to equations (61) and (62). In the TF-limit the energy of a condensate with a central vortex is thus given by

$$\begin{aligned} E_{\text{Tot}} =& N\hbar\omega_\rho \left\{ -\frac{3}{7}\frac{r_{\rho 0}^2}{A_2} - \frac{\beta_0^2 r_{\rho 0}^2}{2} + \frac{\gamma^2 r_{z0}^2(1+\beta_0^2)}{10} + \frac{6\gamma^2 r_{z0}^2}{70 A_2} - \frac{36P}{r_{\rho 0}^2 r_{z0}} \left(\frac{9\beta_0^2}{8A_2} + \frac{1}{2A_2} + \frac{27}{28A_2^2} \right) \right. \\ & \left. + \frac{65}{8 r_{\rho 0}^2 A_2} + \frac{165\beta_0^2}{16 r_{\rho 0}^2 A_2} - \frac{3A_1}{16A_2} \frac{40 + 80\beta_0^2 + 55\beta_0^4}{(1+\beta_0^2) r_{\rho 0}^2} \right\}. \end{aligned} \tag{82}$$

To obtain an analytical expression for the energy we expand equation (82) to fourth order in β and insert our approximate solutions for the equilibrium positions from equations (76)–(78). This leads to

$$\begin{aligned} E_{\text{Tot}} = \frac{N\hbar\omega_\rho}{(P\gamma)^2} & \left\{ 0.184 + 0.185(P\gamma)^{4/5} + 0.622(P\gamma)^{8/5} + 1.055(P\gamma)^{12/5} \right. \\ & + \left[0.351 + 0.707(P\gamma)^{4/5} + 0.339(P\gamma)^{8/5} \right] \ln(P\gamma) \\ & \left. + \left[0.224 - 0.055(P\gamma)^{4/5} \right] \ln^2(P\gamma) + 0.111 \ln^3(P\gamma) \right\}. \end{aligned} \tag{83}$$

In Figure 8 the numerically obtained energy and the approximate analytical solution (83) are plotted against the scattering length a_s for an oblate trap with $\gamma = 5$ and a prolate trap with $\gamma = 0.2$. The agreement of the two curves is excellent. The total energy rises with increasing scattering length as expected, since the part in the energy functional due to the interaction is directly proportional to a_s. However, note that the energy due to the vortex is very small compared to the total energy of the condensate. The energy of a condensate without a vortex in the TF-limit is straightforwardly determined by substituting equation (11) with the relevant radii from (9) and (10) into equation (81) where according to the TF-limit the kinetic energy is neglected. In our rescaled units it turns out to be

$$E_0 = N\hbar\omega_\rho \frac{5}{14} (15P\gamma)^{2/5}. \tag{84}$$

In general it costs energy to create a vortex and if we denote this energy by E_v we may obtain it by substracting E_0 from E_{Tot}

$$E_\text{v} = E_{\text{Tot}} - E_0. \tag{85}$$

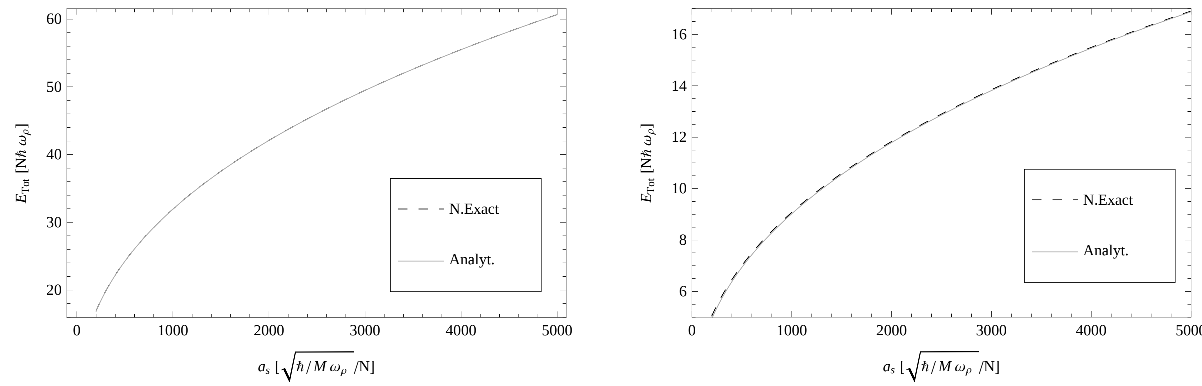

(a) $\gamma = 5$ (b) $\gamma = 0.2$

Figure 8 – The energy of a condensate with a central vortex scaled in units of $N\hbar\omega_\rho$ plotted against the scattering length a_s in an oblate trap (a) and a prolate trap (b). Black dashed curve: Exact numerical solution. Gray solid curve: Approximate analytical solution.

It is possible to stabilize a vortex state by applying a rotating trap potential [23]. To understand this we consider a frame rotating at angular velocity Ω about the z-axis for which the energy of the system becomes

$$E' = E - \Omega L_z. \tag{86}$$

For a nonrotating condensate without angular momentum the energy in the rotating frame remains the same as before, whereas for a condensate with a singly quantized vortex the energy is reduced. This is due to the fact that every particle carries angular momentum of $\hbar$ and consequently the total angular momentum adds up to $L_z = N\hbar$. We see that for a condensate in a trap rotating at angular velocity Ω the vortex state becomes energetically favorable when Ω exceeds a critical rotational frequency at which the energy cost to create a vortex equals the lowering of the energy due to the rotating trap potential. Thus the critical angular frequency becomes

$$\Omega_c = \frac{E_{\text{v}}}{N\hbar}. \tag{87}$$

Inserting the earlier results for the energies from (83) and (84) into (85) and (87) leads to an explicit expression for the critical frequency at which the vortex becomes stable

$$\begin{aligned} \Omega_c = \frac{\omega_\rho}{(P\gamma)^2} \Big\{ & 0.184 + 0.185(P\gamma)^{4/5} + 0.622(P\gamma)^{8/5} \\ & + \left[0.351 + 0.707(P\gamma)^{4/5} + 0.339(P\gamma)^{8/5}\right] \ln(P\gamma) \\ & + \left[0.224 - 0.055(P\gamma)^{4/5}\right] \ln^2(P\gamma) + 0.111 \ln^3(P\gamma) \Big\} . \end{aligned} \tag{88}$$

In Figure 9 the critical rotation frequency Ω_c is displayed as a function of the scattering length a_s for an oblate trap with $\gamma = 5$ and a prolate trap with $\gamma = 0.2$. Here we have plotted the numerical solution, as well as our explicit analytical solution from equation (88). Furthermore an analytical expression for the critical angular velocity obtained by Pethick *et al.* [23] is included in the graphic

$$\Omega_c = \frac{5}{2}\frac{\hbar}{MR_\perp^2}\ln\left(\frac{0.671R_\perp}{\zeta}\right). \tag{89}$$

This result was derived by integrating the kinetic energy density $Mn(\rho,z)v^2(\rho)/2$, arising from the superfluid flow (34) around the vortex, over the profile of the condensate. The lower limit of the integral is set by the coherence length ζ from equation (29) and the density is taken to be the central density for a condensate without a vortex. This approach was already outlined in Section 3.2 to show that higher quantized vortices decay into multiple singly quantized vortices. In our rescaled units equation (89) becomes

$$\Omega_c = \frac{\omega_\rho}{(P\gamma)^2}\left[0.579(P\gamma)^{8/5} + 0.339(P\gamma)^{8/5}\ln(P\gamma)\right]. \tag{90}$$

We see that the leading terms in equations (88) and (90) nearly coincide.
A closer look at Figure 9 reveals that our analytical approximation (88) agrees very well with the numerical result and is indeed consistent with the analytical result derived by Pethick *et al.* from equations (89) and (90). Especially for the prolate trap, it can be seen that our result is even slightly closer to the numerical solution than Pethick's formula.

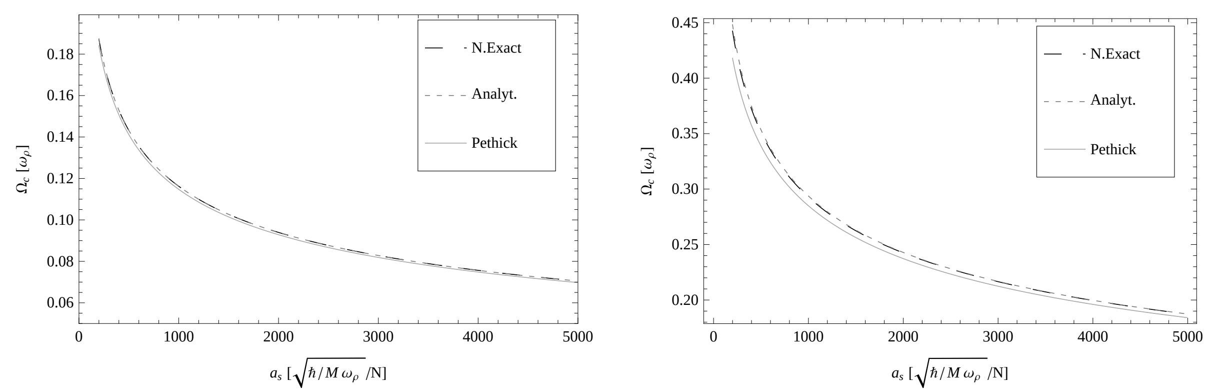

(a) $\gamma = 5$ (b) $\gamma = 0.2$

Figure 9 – The critical angular velocity Ω_c of a rotating trap at which a vortex state becomes energetically favorable is plotted against the scattering length a_s for an oblate trap (a) and a prolate trap (b). Black dashed curve: Exact numerical solution. Gray dashed curve: Approximate analytical solution from equation (88). Gray solid curve: Analytical formula (90) derived by Pethick *et al.* [23].

3.7 Expansion Behavior

An interesting aspect in the investigation of BECs is the question of how a trapped condensate expands after the trapping potential is turned off. This is of utmost importance especially in the context of the experimental detection of vortex states, since the vortex core region is significantly smaller than the radial extension of the condensate and hence difficult to visualize directly.
To investigate the expansion behavior of a condensate with a central vortex after release from the trap, we have to modify the previously obtained equations of motion in such a way that we erase the harmonic oscillator parts $-\gamma^2 r_z(\tau)$ and $-r_\rho(\tau)$ in equations (64) and (65) and the part $15\left[5r_\rho(\tau)^2 - \gamma^2 r_z(\tau)^2\right]$ in equation (66) that is due to the trapping potential, respectively. The resulting equations of motions

$$\begin{aligned}\ddot{r}_z(\tau) =& -\frac{15PA_4(\tau)}{2(A_3(\tau)-15)r_\rho(\tau)^2 r_z(\tau)^2} + \frac{4\beta(\tau)A_7(\tau)\dot{r}_z(\tau)\dot{\beta}(\tau)}{A_3(\tau)-15} \\ &+ \frac{2\left(15+A_7(\tau)\right)r_z(\tau)\dot{\beta}(\tau)^2}{A_3(\tau)-15} - \frac{4\beta(\tau)^2 A_7(\tau)^2 r_z(\tau)\dot{\beta}(\tau)^2}{15\left[A_3(\tau)-15\right]} \\ &+ \frac{2\beta(\tau)A_7(\tau)r_z(\tau)\ddot{\beta}(\tau)}{A_3(\tau)-15},\end{aligned} \tag{91}$$

$$\begin{aligned}\ddot{r}_\rho(\tau) =& \frac{35A_9(\tau)}{24[6+A_3(\tau)]r_\rho(\tau)^3} \\ &+ \frac{3A_4(\tau)P}{[6+A_3(\tau)]r_\rho(\tau)^3 r_z(\tau)} + \frac{2A_7(\tau)^2\beta(\tau)^2 r_\rho(\tau)^2\dot{\beta}(\tau)^2}{3[6+A_3(\tau)]} \\ &+ \frac{2[15+A_7(\tau)]r_\rho(\tau)\dot{\beta}(\tau)^2}{6+A_3(\tau)} + \frac{2A_7(\tau)\beta(\tau)[2\dot{r}_\rho(\tau)\dot{\beta}(\tau)+r_\rho(\tau)\ddot{\beta}(\tau)]}{6+A_3(\tau)},\end{aligned} \tag{92}$$

$$\begin{aligned}\ddot{\beta}(\tau) =& \left(\frac{7875}{4A_7(\tau)\beta(\tau)^2 r_\rho(\tau)^2} - r_z(\tau)\left[15\ddot{r}_z(\tau) + 4A_7(\tau)\beta(\tau)\dot{\beta}(\tau)\dot{r}_z(\tau)\right] - \frac{875A_8(\tau)}{8A_7(\tau)r_\rho(\tau)^2}\right. \\ &+25r_\rho(\tau)\left[3\ddot{r}_\rho(\tau) - 2A_7(\tau)\beta(\tau)\dot{\beta}(\tau)\dot{r}_\rho(\tau)\right] \\ &\left.\frac{225P\left\{-409+120\ln\left[2/\beta(t)\right]\right\}}{2A_7(\tau)r_z(\tau)r_\rho(\tau)^2}\right)/A_7(\tau)\beta(\tau)\left[25r_\rho(\tau)^2+2r_z(\tau)^2\right],\end{aligned} \tag{93}$$

are essentially the same that we would have obtained if we had not included the trapping potential in the Lagrange function before extremizing the action. We now solve these equations numerically for an oblate trap with $\gamma = 5$ and a prolate trap with $\gamma = 0.2$ and take as initial conditions the numerically determined equilibrium positions for a trapped condensate from Section 3.5 and zero velocities.
In a previous study [24] it has been suggested that the vortex core radius expands faster than the radial extension of the cloud, which makes experimental detection feasable by using a time-of-flight method, where the condensate is first set free and then pictures are taken after a short time of expansion. Figure 10 shows the evolution of the ratio of the vortex core

size to the radial extension of the cloud $\beta = \xi/R_\rho$ in time. Indeed, this ratio increases and especially for an oblate trap and a high scattering length the vortex core radius grows rapidly in time. This is an important insight for the experimental detection and the investigation of vortex states. Hence, our study qualitatively confirms the result from Ref. [24] which was obtained with a different trial function. Note that we have only plotted the graph until β reaches 0.15 as our assumption for β to be small begins to break down.

Another quantity of interest is the aspect ratio of the condensate and its evolution in time after the release from the trap. In noncondensed sytems the gaseous cloud always strives towards an isotropic density distribution and, consequently, the aspect ratio tends to unity no matter what it was in the trapped state. In the case of trapped BECs, however, an aspect ratio inversion takes place. This represents a phenomenon which is impossible in classical systems, and, therefore, a characteristic of quantum behavior.

Figure 11 displays the radial and axial free expansion in time. The aspect ratio inversion is clearly visible and the aspect ratio is unity as the curves for both directions cross each other. The gradient of the curves suggests that, after an initial stage, the expansion in the different directions develops with constant velocity.

Recently it was observed in an experimental study [25] that in turbulent condensates with tangeled vortex configurations, the aspect ratio inversion is suppressed and the ratio stays constant during the free expansion. However, for a single vortex we cannot confirm this tendency. In Figure 12 we have depicted the dynamical change of the aspect ratio κ for a condensate with and without a vortex. The curve for a condensate without a vortex is determined by numerically solving the equations of motion obtained from an analogous variational principle with a different trial function

$$\psi(\rho, z, t) = C\sqrt{1 - \left[\frac{\rho}{R_\perp(t)}\right]^2 - \left[\frac{z}{R_\parallel(t)}\right]^2}\,\mathrm{e}^{iB_\perp(t)\rho^2 + iB_\parallel(t)z^2}, \tag{94}$$

which corresponds to the Thomas-Fermi approximation. For both curves Figure 12 clearly depicts the aspect ratio inversion with little difference between the curves. Therefore, we conclude that a single vortex does not affect the global expansion of the condensate significantly and measuring the aspect ratio after free expansion does not provide an effective mean to detect single vortex states.

In Figure 13 a density plot of the condensate in the trapped state and after turning off the trapping potential is depicted. The vortex core region is clearly visible as a bright line and its width increases in time, faster than the radial extension.

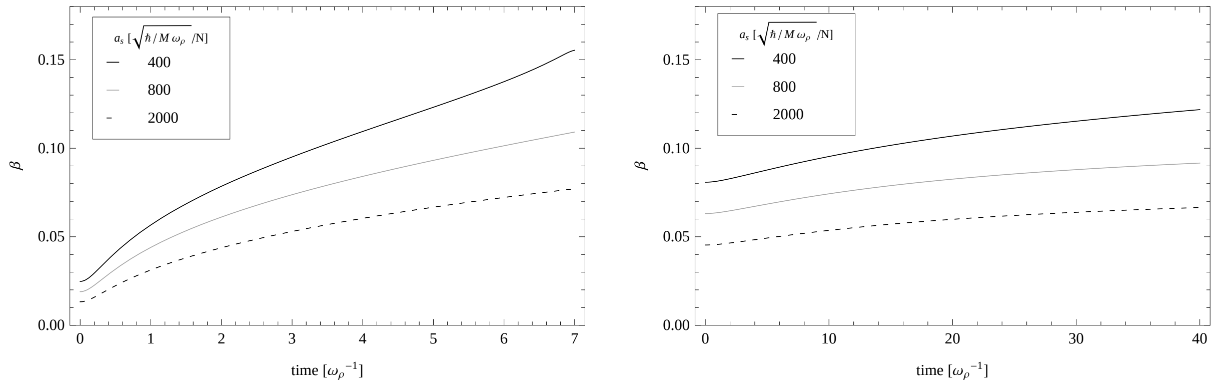

(a) $\gamma = 5$ (b) $\gamma = 0.2$

Figure 10 – Evolution in time of the ratio of the vortex core radius to the total radial extension $\beta = \xi / R_\rho$ after turning off the trapping potential in an oblate trap (a) and a prolate trap (b) for different scattering lengths a_s.

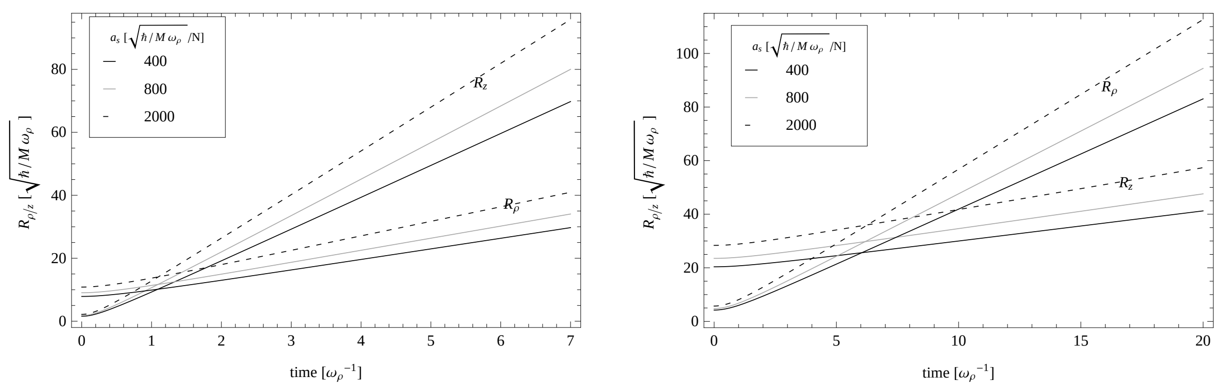

(a) $\gamma = 5$ (b) $\gamma = 0.2$

Figure 11 – Evolution in time of the spatial extensions R_ρ and R_z of the system after turning off the trapping potential in an oblate trap (a) and a prolate trap (b) for different scattering lengths a_s.

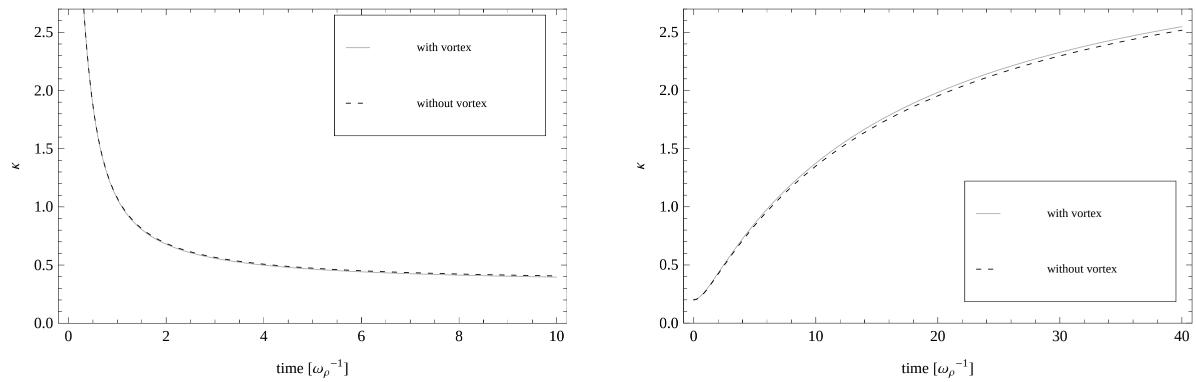

(a) $\gamma = 5$ (b) $\gamma = 0.2$

Figure 12 – Evolution in time of the aspect ratio κ of the condensate after turning off the trapping potential in an oblate trap (a) and a prolate trap (b) for different scattering lengths a_s.

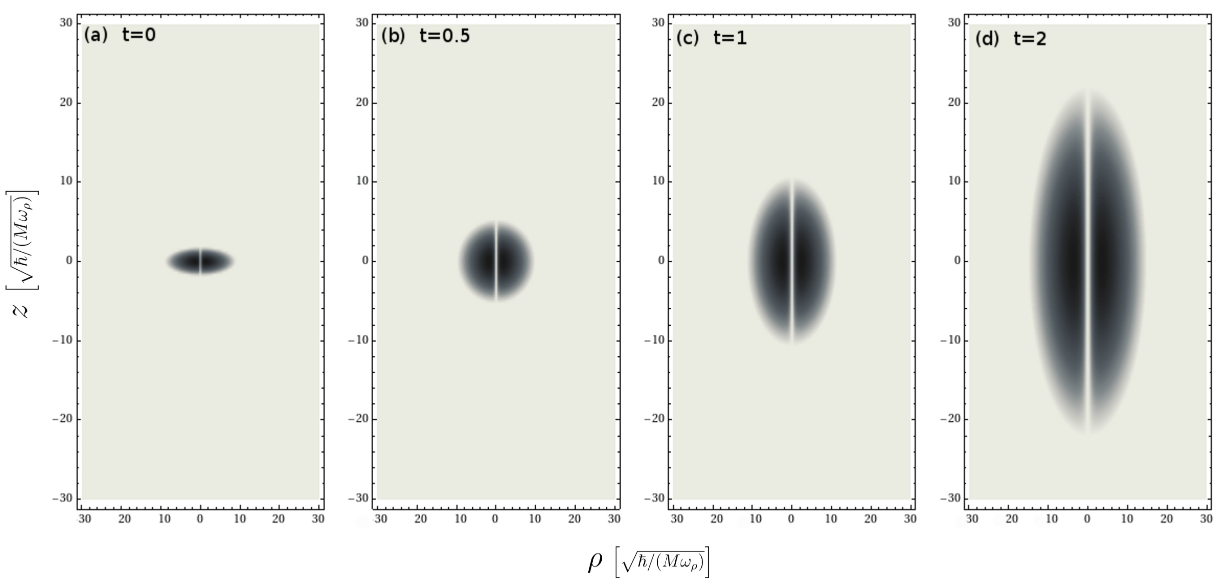

Figure 13 – Density profiles of an expanding condensate with a central vortex after turning off the trapping potential. Time is measured in units of ω_ρ^{-1}. The scattering length is $a_s = 800\sqrt{\frac{\hbar}{M\omega_\rho}}/N$ and the ratio of the trap frequencies before turning off the potential was $\gamma = 5$.

4 Discussion and Outlook

In this work we studied a Bose-Einstein condensate with a central vortex using a variational approach. We have derived approximate equations of motion (64)–(66) for variational parameters that describe the spatial extensions R_ρ and R_z and the ratio β of the vortex core size to the radial extension of the condensate. We then studied the equilibrium positions of the condensate and, apart from numerical solutions, we also found approximate analytical expressions for the stationary points of the system (76)–(78). Thereby we discovered that the spatial extensions of the cloud do not significantly differ from those of a condensate without a vortex. All numerical results are in excellent agreement with previous studies [12].
In Section 3.6 we have found analytical formulas for the energy (83) of a condensate with a central vortex and in equation (88) for the critical frequency Ω_c of a rotating trap at which the vortex state becomes stable. This result was crosschecked by numerical calculations and furthermore compared to a formula for Ω_c derived by Pethick *et al.* [23], with which it was in very good quantitative agreement.
In Section 3.7 we have analysed the free expansion behavior of a previously trapped condensate with a central vortex and confirmed the proposition made in previous studies [24], that in free expansion the vortex core radius expands relatively faster than the radial extension of the cloud. This is an important insight for both the experimental detection and the visualization of vortex states.

In a prior attempt we utilized a different trial function in our variational approach, namely

$$\psi(\rho, z, \varphi, t) = C(t) \exp\left\{ i\varphi + \left[\frac{1}{2R_\rho(t)^2} + iB_\rho(t)\right]\rho^2 + \left[\frac{1}{2R_z(t)^2} + iB_z(t)\right] z^2 - \frac{\xi(t)^2}{\rho^2} \right\}. \tag{95}$$

This choice was motivated by the successful investigation of the dynamics of a BEC without a vortex via a Gaussian trial function [20]. However, it turned out to be that, within our range of investigated scattering lengths, the vortex state was energetically favorable even when no rotating trap potential was applied which is physically illegitimate. The reason is that the use of a Gaussian trial function is only appropriate in the weak-coupling limit as the GP equation then reduces to a regular Schrödinger equation for which in case of an harmonic trap potential the ground state wave function is Gaussian. Since we were interested in the opposite case, namely the TF limit where the interaction energy dominates the kinetic energy leading to small vortex core sizes, we had to use a different trial function, and, therefore, we chose our trial function to be of the form (36).

A possible continuation of this work would be to study the collective excitations of the condensate and the corresponding normal modes and oscillation frequencies. This could then be compared to theoretical studies approaching this issue not via a variational approach, but by a more direct investigation of the Gross-Pitaievski equation via a Bogoliubov-de Gennes analysis [26]. Furthermore, the whole physical questioning could be generalized to the study of off-axis vortices. Topics of interest could then be the phenomenon of vortex bending due to symmetry breaking as well as the investigation of precession frequencies, which can be interpreted as collective excitations [13].

The Feshbach resonance technique, which enables a variation of the scattering length via a magnetic field, is one of the most promising tools for manipulating the properties of BECs and has been investigated experimentally and theoretically to excite collective modes. As vortex states are in fact a collective excitation of the condensate it could be futile to investigate if a vortex state could be stabilized or destabilized by this technique. This would correspond to replace the rescaled interaction strength P by $P \to P(\tau) = P_0 + P_1 \cos(\Omega\tau)$ in the equations of motion (65)–(66). In Ref. [27] a first step in this direction has been made, as the possibility to stabilize a vortex state via modulation of the scattering length is demonstrated in a uniform condensate. However, this seems to be possible only for an attractive interaction which corresponds to P_0 being negative. For a harmonic trap it has been shown by Bagnato *et al.* that the vortex mode cannot be excited by a modulation of the scattering length [28], but it remains possible that employing a nonsymmetric trapping potential would make the generation of the vortex state possible. An investigation of our equation of motions (65)–(66) with a periodically modulated interaction strength P might still be worthwhile since the study in Ref. [28] was done in the weak-coupling regime whereas our study is carried out in the strong-coupling TF limit.

References

[1] S. N. Bose. Plancks Gesetz und Lichtquantenhypothese. *Z. Phys.*, 26:178, 1924.

[2] A. Einstein. Quantentheorie des einatomigen idealen Gases - Zweite Abhandlung. *Sitz. Ber. Preuss. Akad. Wiss.*, 22:261, 1924.

[3] S. Cornell, C. Wieman, M. Matthews, M. Anderson, and J. Ensher. Observation of Bose-Einstein Condensation in a Dilute Atomic Vapor. *Science*, 269:198, 1995.

[4] K. B. Davis, M. O. Mewes, M. R. Andrews, N. J. van Druten, D. S. Durfee, D. M. Kurn, and W. Ketterle. Bose-Einstein Condensation in a Gas of Sodium Atoms. *Phys. Rev. Lett.*, 75(22):3969–3973, 1995.

[5] E. P. Gross. Structure of a Quantized Vortex in Boson Systems. *Il Nuovo Cimento*, 20(3):454, 1961.

[6] L. P. Pitaevskii. Vortex Lines in an Imperfect Bose Gas. *Sov. Phys. JETP-USSR*, 13(2):451–454, 1961.

[7] M. Tsubota, K. Kasamatsu, and M. Kobayashi. Quantized Vortices in Superfluid Helium and Atomic Bose-Einstein Condensates. `arXiv:1004.5458v2`, 2010.

[8] M. R. Matthews, B. P. Anderson, P. C. Haljan, D. S. Hall, C. E. Wieman, and E. A. Cornell. Vortices in a Bose-Einstein Condensate. *Phys. Rev. Lett.*, 83:2498–2501, 1999.

[9] F. Chevy, K. W. Madison, and J. Dalibard. Measurement of the Angular Momentum of a Rotating Bose-Einstein Condensate. *Phys. Rev. Lett.*, 85:2223–2227, 2002.

[10] E. Hodby, G. Hechenblaikner, S. A. Hopkins, O. M. Maragò, and C. J. Foot. Vortex Nucleation in Bose-Einstein Condensates in an Oblate, Purely Magnetic Potential. *Phys. Rev. Lett.*, 88(1):010405, 2001.

[11] V. Bretin, P. Rosenbusch, F. Chevy, G. V. Shlyapnikov, and J. Dalibard. Quadrupole Oscillation of a Single-Vortex Bose-Einstein Condensate: Evidence for Kelvin Modes. *Phys. Rev. Lett.*, 90(10):100403, 2003.

[12] D. H. J. O'Dell and C. Eberlein. Vortex in a Trapped Bose-Einstein Condensate with Dipole-Dipole Interactions. *Phys. Rev. A*, 75(1):013604, 2007.

[13] Anatoly A. Svidzinsky and A. L. Fetter. Stability of a Vortex in a Trapped Bose-Einstein Condensate. *Phys. Rev. Lett.*, 84(26):5919–5923, 2000.

[14] K. W. Madison, F. Chevy, W. Wohlleben, and J. Dalibard. Vortex Formation in a Stirred Bose-Einstein Condensate. *Phys. Rev. Lett.*, 84(5):806–809, 2000.

[15] S. Stringari. Phase Diagram of Quantized Vortices in a Trapped Bose-Einstein Condensed Gas. *Phys. Rev. Lett.*, 82(22):4371–4375, 1999.

[16] K. Huang. *Statistical Mechanics.* 2nd ed., Whiley, 1987.

[17] R. J. Donnelly. *Quantized Vortices in Helium II.* Cambridge University Press, 1991.

[18] L. Onsager. Statistical Hydrodynamics. *Il Nuovo Cimento*, 6:249, 1949.

[19] S. Stringari. Collective Excitations of a Trapped Bose-Condensed Gas. *Phys. Rev. Lett.*, 77:2360, 2000.

[20] V. M. Perez-Garcia, H. Michinel, J. I. Chirac, M. Lewenstein, and P. Zoller. Dynamics of Bose-Einstein Condensates: Variatonal Solutions of the Gross-Pitaevskii Equations. *Phys. Rev. A.*, 56:1424, 1997.

[21] G. Baym and C. J. Pethick. Ground-State Properties of Magnetically Trapped Bose-Condensed Rubidium Gas. *Phys. Rev. Lett.*, 76(1):74, 1995.

[22] J. Werner, A. Griesmaier, S. Hensler, J. Stuhler, T. Pfau, A. Simoni, and E. Tiesinga. Observation of Feshbach Resonances in an Ultracold Gas of ^{52}Cr. *Phys. Rev. Lett.*, 94(18):183201, 2005.

[23] E. Lundh, C. J. Pethick, and H. Smith. Zero-Temperature Properties of a Trapped Bose-Condensed Gas: Beyond the Thomas-Fermi Approximation. *Phys. Rev. A*, 55(3):2126–2131, 1997.

[24] E. Lundh, C. J. Pethick, and H. Smith. Vortices in Bose-Einstein-Condensed Atomic Clouds. *Phys. Rev. A*, 58(6):4816–4823, 1998.

[25] E. A. L. Henn, J. A. Seman, G. Roati, K. M. F. Magalhaes, and V.S. Bagnato. Generation of Vortices and Observation of Quantum Turbulence in an Oscillating Bose-Einstein Condensate. *Low Temperature Physics*, 158:435–442, 2010.

[26] R. J. Dodd, K. Burnett, M. Edwards, and C. W. Clark. Excitation Spectroscopy of Vortex States in Dilute Bose-Einstein Condensed Gases. *Phys. Rev. A*, 56(1):587–590, 1997.

[27] S. K. Adhikari. Stabilization of Bright Solitons and Vortex Solitons in a Trapless Three-Dimensional Bose-Einstein Condensate by Temporal Modulation of the Scattering Length. *Phys. Rev. A*, 6(6):063613, 2004.

[28] E. R. F. Ramos, E. A. L. Henn, J. A. Seman, M. A. Caracanhas, K. M. F. Magalhães, K. Helmerson, V. I. Yukalov, and V. S. Bagnato. Generation of Nonground-State Bose-Einstein Condensates by Modulating Atomic Interactions. *Phys. Rev. A*, 78(6):063412, 2008.

Commitment

This is to certify that I wrote this work on my own and that the references include all the sources of information I have utilised.

Berlin, August 11th 2010 Nikolas Zöller